SARS-CoV-2 Omicron Variant Binds to Human Cells More Strongly than Wild Type: Evidence from Molecular Dynamics Simulation

Hoang Linh Nguyen, Quoc Thai Nguyen, Phuong H Nguyen, Mai Suan Li

SARS-CoV-2 Omicron Variant Binds to Human Cells More Strongly than Wild Type: Evidence from Molecular Dynamics Simulation

Hoang Linh Nguyen[1,2,3], Nguyen Quoc Thai[1,4], Phuong H. Nguyen[5] and Mai Suan Li[6,*]

[1]Life Science Lab, Institute for Computational Science and Technology, Quang Trung Software City, Tan Chanh Hiep Ward, District 12, Ho Chi Minh City, Vietnam

[2]Ho Chi Minh City University of Technology (HCMUT), Ho Chi Minh City 700000, Vietnam

[3]Vietnam National University, Ho Chi Minh City 700000, Vietnam

[4]Dong Thap University, 783 Pham Huu Lau Street, Ward 6, Cao Lanh City, Dong Thap, Vietnam

[5]CNRS, Universit´e de Paris, UPR9080, Laboratoire de Biochimie Th´eorique, Paris,France ; Institut de Biologie Physico-Chimique, FondationEdmond de Rothschild, PSLResearch University, Paris, France

[6]Institute of Physics, Polish Academy of Sciences, al. Lotnikow 32/46, 02-668, Warsaw, Poland

*Email: masli@ifpan.edu.pl

Abstract

The emergence of the variant of concern Omicron (B.1.1.529) of the severe acute respiratory syndrome coronavirus 2 (SARS-CoV-2) aggravates the covid-19 pandemic due to its very contagious ability. The high infection rate may be due to the high binding affinity of Omicron to human cells, but both experimental and computational studies have yielded conflicting results on this issue. Some studies have shown that the Omicron variant binds to human angiotensin-converting enzyme 2 (hACE2) more strongly than wild type (WT), but other studies have reported comparable binding affinities. To shed light on this open problem, in this work, we calculated the binding free energy of the receptor binding domain (RBD) of the WT and Omicron spike protein to hACE2 using all-atom molecular dynamics simulation and molecular mechanics Poisson-Boltzmann surface area (MM-PBSA) method. We showed that Omicron binds to human cells more strongly than WT due to increased RBD charge, which enhances electrostatic interaction with negatively charged hACE2. N440K, T478K, E484A, Q493R and Q498R mutations in RBD have been found to play a critical role in the stability of the RBD-hACE2 complex. The effect of homogeneous and heterogeneous models of glycans coating the viral RBD and the peptidyl domain (PD) of hACE2 was examined. Although the total binding free energy is not sensitive to the glycan model, the distribution of per-residue interaction

energies depends on it. In addition, glycans have little effect on the binding affinity of WT RBD to hACE2.

Keywords: Omicron variant, COVID-19, SARS-CoV-2, glycans, spike protein, human angiotensin-converting enzyme 2, receptor binding domain, peptidyl domain, MM-PBSA, binding free energy

Introduction

The coronavirus disease (COVID-19) pandemic caused by severe acute respiratory syndrome coronavirus 2 (SARS-CoV-2)[1] has killed more than 5.5 million people out of over 313 million confirmed cases worldwide[2]. SARS-CoV-2 is a new member of the beta genera of genus coronavirus[1]. The virion comprises of a single positive-strand RNA enveloped by a lipid bilayer with spherical like shape. Among various virial proteins, the so-called spike (S) protein protruding from the lipid bilayer plays an important role in the invasion of host cells as well as in antibody binding[3-7]. Binding of the receptor binding domain (RBD) of the S protein to the human Angiotensin-converting enzyme 2 (hACE2) protein initiates entry of the virus to the host cell [8,9].

In November 2021, a newly emerging variant called Omicron (B.1.1.529) was reported as a variant of concern[10]. This variant encodes a large number of genomic mutations including 32 mutations in the spike protein[11] (Table 1). The outbreak of the Delta variant has unleashed a devastating wave of the pandemic[12-14], but Omicron makes the virus spread even faster, bringing a lot of attention to its dominant role [15]. Therefore, understanding the molecular mechanism underlying the interaction of Omicron with hACE2 is very important as it may shed light on the high transmissibility of this variant. A large number of mutations in the S protein are expected to drastically change this interaction, but different groups have reported conflicting experimental results. The binding affinity of the Omicron variant S protein to hACE2 was found to be higher (lower the dissociation constant K_D) than that of the SARS-CoV-2 wild-type (WT) analog [16,17] (Table 2). However, Wu *et al.* reported this binding affinity is comparable to WT[18]. Chan *et al.* [19] obtained K_D = 22 nM, which suggests that WT and Omicron have almost the same binding affinity if this value is compared to K_D of Omicron from Cameroni *et al* [16] and Wu *et al.* [18]

(Table 2). However, when this KD value is compared with that of Zhang *et al.* [17], Omicron binds more closely to hACE2.

Computational studies have also produced conflicting results. Using an artificial intelligence model and docking simulation, it was shown that Omicron is more contagious than the WT virus[20,21]. Omotuyi *et al.* performed molecular dynamics (MD) simulations showing that Omicron exhibits a stronger interaction with hACE2[22], but binding free energy has not been reported. However, the comparable binding affinity was obtained [18] combining MD modeling with the molecular mechanics Poisson-Boltzmann surface area (MM-PBSA) method.

Since both experimental and computational results are inconsistent with each other, here we attempted to calculate the binding free energy of WT and the Omicron variant of SARS-CoV-2 interacting with hACE2 using the MM-PBSA method. In contrast to previous works [18] our all-atom model includes glycans flanked around the RBD of S protein. We have shown that the Omicron RBD binds to the peptidyl domain (PD) of hACE2 more strongly than WT.

In both implemented glycan models, electrostatic interaction prevails over the van der Waals (vdW) interaction in binding of WT and Omicron to human cells. In addition, Omicron displays a stronger electrostatic interaction with hACE2 than WT.

We determined three interface regions between the RBD and hACE2 PD. The mutations help Omicron improve the interaction with hACE2 compared to WT in two interface regions, while in the other region Omicron has a weaker interaction with hACE2, which suggests that the SARS-CoV-2 virus still has room to improve its binding human cells.

We have identified three interface regions between RBD and hACE2 PD. The mutations help Omicron to improve interaction with hACE2 compared to WT in two interface regions, while in another region Omicron has weaker interaction with hACE2, suggesting that SARS-CoV-2 still has room for improved binding affinity with human cells.

Finally, our MD simulation without glycans showed that glycans have insignificant effect on the binding free energy of RBD WT to hACE2 PD.

Materials and methods

Molecular dynamics simulation

The RBD structure of the SARS-CoV-2 S protein complexed with the hACE2 PD was obtained from the Protein Data Bank (PDB) with PDB id 6LZG [23]. The missing residues of this WT structure were added by the CHARMM-GUI webserver. Four glycans are located at residues 53, 90, and 322 of the hACE2 PD and at residue 343 of the viral RBD. In this work, we adopted two glycan schemes that were created using the CHARMM-GUI web server. In a homogeneous setup, all glycans are of the same type, while in a heterogeneous setup, glycan sites have different glycans [24,25]. The Omicron variant was generated from WT RBD using the CHARMM-GUI webserver. In total we have 4 complexes with 2 sets of glycans for each variant. The Zn ion in hACE2 PD of the original structure was retained. The original structures for WT and Omicron are shown in Figure 1. All mutations of Omicron are presented in Figure S1 in Supporting Information (SI).

The AMBER19SB and GLYCAM06j force fields were used to describe proteins and glycans[26,27]. The systems were solvated in a rectangular box filled with 4-points OPC water molecules with a minimum distance of 1.3 nm from the solute to the edge of the box [28]. To neutralize the system, Na^+ and Cl^- ions were added, maintaining the salt concentration at the physiological level of 0.15 M.

The GROMACS 2021.3 package was used for MD simulation. The solvated systems were minimized by a steep descent algorithm for structure relaxation. The system was then equilibrated in NVT and then in NPT ensembles at 300 K and 1 atm for 500 ps and 5 ns MD runs, respectively. The v-rescale and Parrinello-Rahman algorithms were utilized to keep constant temperature and pressure, respectively[29,30]. At the equilibration stage, the heavy atoms of the protein-glycan complexes were restrained by a harmonic potential with a spring constant k =1000kJ/mol/nm.

To estimate the binding free energy by the MM-PBSA method, for each system, 5 independent MD trajectories with a duration of 200 ns were carried out without restraints at 300 K and 1 atm. We used a cutoff of 1.0 nm for non-bonded interactions. The PME method was used to calculate the electrostatic interaction[31].

MM-PBSA method

In the MM-PBSA method, the binding free energy was obtained using the following equation:

$$\Delta G_{bind} = \Delta E_{elec} + \Delta E_{vdW} + \Delta G_{polar} + \Delta G_{nonpolar} - T\Delta S$$

Here ΔE_{elec} and ΔE_{vdW} are the energies of the electrostatic and vdW interactions, and ΔG_{polar} is the polar solvation energy, which is calculated using the Delphi software[32]. The non-polar solvate energy $\Delta G_{nonpolar} = \gamma\Delta SASA$, where $\gamma = 0.0072$ kcal/mol/nm^2, and SASA is solvent accessible surface area calculated using gmx sasa tool in the GROMACS package with a solvent probe radius of 1.4 Å[33]. The entropy contribution $T\Delta S$ was evaluated according to the method proposed by Duan et al[34].

Hydrogen bond

A hydrogen bond is formed if the distance between donor D and acceptor A is less than 0.35 nm, the H-A distance is less than 0.27 nm, and the D-H-A angle is larger than 135^0.

Side-chain contact

A contact between two residues is formed when the distance between the centers of mass of their sidechains is ≤ 6.5 Å.

Results and discussions

Omicron variant has higher binding affinity than wild type

Root mean square displacement (RMSD) relative to the initial structure was calculated using the atomic coordinates of Cα atoms of the S protein RBD and hACE2 PD. Its time dependence shows that all complexes reached equilibrium after 100 ns (Figures S2 and S3). Therefore, the snapshots collected over the last 100 ns of MD simulation were used for data analysis.

Using MM-PBSA method, we obtained the binding free energy ΔG_{bind} of WT and Omicron RBD interacting with hACE2 PD with two glycan models (Table 3). In the case of a homogeneous glycan setup, Omicron has ΔG_{bind} (-30.21 ± 5.48 kcal/mol) lower than that of WT (-18.32 ± 1.62 kcal/mol). This result indicates that the Omicron variant binds to hACE2 more strongly than WT, which is consistent with the experiment of Cameroni *et al* and Zhang *et al*[16,17]. This conclusion remains also valid for the heterogeneous glycan setup (Table 3).

Experiments showed that K_D of RBD-PD complexes falls in the nM range (Table 1), which corresponds to ΔG_{bind} ~ -12 kcal/mol. Therefore, the absolute value of the binding free energy predicted by the MM-PBSA method is much larger than the experimental value, implying that this method is good for evaluating the relative binding free energies, but not their absolute value. The same has been mentioned in previous works [35,36]. By combining coarse-grained models [37] with umbrella sampling, reasonable results can be obtained for the absolute value of ΔG_{bind} and K_D [38], but coarse-grained modeling is not sensitive enough to describe effects of mutations.

Using the same MM-PBSA method and AMBER19SB force field, Wu *el al* [18] showed that WT and Omicron have comparable binding affinities, contradicting our results. Here are some of the reasons for this difference: we used the 4-point OPC water model, while Wu et al. used TIP3P; we took into account glycans that were neglected by Wu et al.

Electrostatic interaction plays a crucial role in the stability of the RBD-PD complex

The electrostatic interaction dominates over the vdW interaction in all complexes of hACE2 and SARS-CoV-2 RBD (Table 3). For the WT and homogeneous glycan model, E_{elec} = -856 kcal/mol, which much less than E_{vdW} = -152 kcal/mol. For the Omicron variant, the role of the electrostatic interaction becomes even more pronounced, because for the same glycan model we have E_{elec} = - 1645 kcal/mol and E_{vdW} = -145 kcal/mol (Table 3). This conclusion is also valid for the heterogeneous glycan model. The dominant role of the electrostatic interaction is related to the fact that both PD of hACE2 and RBD are charged. The charge of hACE2 PD is -27e, while the charge of WT RBD is +3e and of Omicron RBD is +6e. Thus, the higher binding affinity of Omicron is due to the increased attractive electrostatic interaction.

Impact of glycan model on the interaction energy between RBD and hACE2 PD

We divided the interaction energies between the viral RBD and hACE2 PD into protein and glycan parts (Table S1). In both glycan models, the energy contribution of proteins dominates over glycans.

In the homogeneous glycan model, hACE2 glycans have a stronger vdW interaction with WT RBD (-42.88 kcal/mol) than Omicron (-10.34 kcal/mol) (Table S1, Figure 2). The electrostatic interaction between hACE2 glycans and Omicron RBD glycans is repulsive (41.59 kcal/mol), while hACE2 glycans have an attractive electrostatic interaction with the WT RBD glycans (-

12.36 kcal/mol) (Table S1, Figure 2). The interaction energy of RBD glycans with hACE2 protein (≈ 50 kcal/mol) is higher than that of WT glycans (≈ 4 kcal/mol) (Table S1, Figure 2), which implies that RBD glycans reduces the binding affinity of Omicron to a greater extent than WT.

In the case of the heterogeneous glycan model, the interaction energies between RBD and hACE2 glycans are equivalent within errors for WT and Omicron (Table S1, Figure 2). Similarly, the difference in interactions between RBD glycans and hACE2 protein is insignificant for WT and Omicron. The interaction energy between RBD and hACE2 glycans is larger than in the homogeneous model (Table S1, Figure 2). The protein part of Omicron RBD has a significantly lower non-bonded interaction energy with hACE2 glycans (-465 kcal/mol) than WT (-230 kcal/mol) (Figure 2). These results suggest that the influence of glycan models on specific components of the interaction energy between RBD and hACE2 is important. However, the effect of glycan models on the difference in the binding affinity of SARS-CoV-2 variants to hACE2 is insignificant (Table 3).

We calculated the percentage of SASA of glycans in relation to the total SASA (Table S2). The area covered by hACE2 glycans in the Omicron case is clearly larger than WT in both glycosylation models. However, RBD glycans the same coverage in both variants, which is probably due to the fact that RBD has only one glycosylation site at residue N343. Thus, the Omicron variant strongly alters the orientation of glycan molecules of hACE2 but not RBD. This is in line with Mehdipour *et al.* who reported that hACE2 glycans play a prominent role in the interaction between viral RBD and hACE2[39].

Important residues in binding of viral RBD and hACE2 PD: Strong effect of glycan models and importance of electrostatic interaction

We calculated the contribution of RBD residues to the interaction energy with hACE2 for WT and Omicron (Figure 3). Residues that have an absolute value of the interaction energy ≥ 150 kcal/mol are listed in Table 4 and their positions are shown in Figure S4. Glycan models have a noticeable effect on the per-residue distribution of interaction energies (Figure 3). In the homogeneous glycan model the number of RBD residues that have an interaction energy below -150 kcal/mol is 26 for WT and 18 for Omicron, while in the heterogeneous model these numbers

are 18 and 21 (Table 4). The number of residues with an interaction energy exceeding 150 kcal/ mol is also different for the two glycan models.

To investigate the effect of mutations in Omicron, the difference between the per-residue energies of Omicron and WT ($E_{\text{Omicron}} - E_{\text{WT}}$) was calculated (Figure 4). In the homogeneous glycan model, the difference between WT and Omicron is seen for many RBD residues with large energy fluctuations. However, in the heterogeneous model, the energy difference has a sharp peak at a much lower number of mutations, again showing that the glycan model drastically affects the interaction energies of RBD with hACE2 across residues.

For the homogeneous glycan model, not only mutated residues but also other RBD residues contribute to the different stability of WT and Omicron (Figure 4). Mutations G339D, K417N, G446S, and G496S destabilize the complex, while S373P, N440K, T487K, E484A, Q493R, Q498R, and Y505H stabilize it, highlighting the importance of mutations that change charge. Namely, G339D and K417N reduce the net charge, resulting in a weaker interaction between Omicron and hACE2. In contrast, N440K, T487K, E484A, Q493R, Q498R, and Y505H increase the total charge promoting an attractive interaction of RBD with the negatively charged hACE2.

In the heterogeneous glycan model, the pattern of per-residue interaction energies is much simpler than the homogeneous case (Figure 4). Interestingly, only the mutated residues in RBD play a primary role in the energy difference between WT and Omicron. As in the homogeneous setup the mutations G339D and K417N weaken the interaction between RBD and hACE2 by increasing the non-bonded interaction energy in Omicron compared to WT. In addition, mutations N440K, T478K, E484A, Q493R, Q498R enhance the binding affinity, but the mutations S371L, S373P, S375F, G446S, S477N, G496S, N501Y, and Y505H have a negligible effect. The effect of G339D and K417N mutations on the binding energy is less than that caused by N440K, T478K, E484A, Q493R, Q498R mutations leading to the stronger binding of Omicron to hACE2.

Important residues at the RBD-hACE2 interface

To investigate the contribution of residues located at the RBD-hACE2 interface to the complex stability we calculated the interaction energy of RBD residues that form sidechain contact with hACE2. In the homogeneous glycan model, the number of these residues are 20 and 18 for WT

and Omicron, respectively (Figure S5). For the heterogeneous setup, we have 25 and 19 residues for WT and Omicron, respectively. Using snapshots from the last 100 ns of MD simulation, we can show that the population of side chain contacts formed by these residues with hACE2 varies from a few % to ≈ 50% (Figure S5). This population is sensitive to glycan models, but is generally greater for Omicron than for WT, implying a higher binding affinity of Omicron.

For clarity we divide these residues into red, green and yellow regions as shown in Figures 5 and 6 (see also Figure S5). With the homogeneous glycan model, the contribution of these regions to the total energy is -212.38 and -508.15 kcal/mol for WT and Omicron, respectively. In the heterogeneous glycan scheme, these contributions are -202.84 and -870.43 kcal/mol. Therefore, the contribution of the interface area to the stability of RBD-hACE2 stability is significant.

For the homogenous glycan model, the red region of Omicron (Figure 5) has a weaker interaction with hACE2 (-71.20 kcal/mol) compared to WT (-217.85 kcal/mol) (Table 5). This effect corresponds to a decrease of hydropathy index from 3.1 for WT to -2.1 for Omicron (Table 5), indicating that the red region of WT is more hydrophobic than Omicron. In particular, the S477N mutation attenuates the interaction between RBD and hACE2 from -58.81 (WT) to -17.04 kcal/mol (Omicron) (Figure 5). In the green region, the mutation Q493R dramatically increases the interaction between the two molecules from 128.39 (WT) to -356.90 kcal/mol (Omicron). This effect occurs because the R amino acid has a positive charge (+e) while the Q amino acid is neutral. In contrast, the G496S mutation weakens the interaction (Figure 5). L455 is not mutated but in WT this residue has a lower interaction energy than in Omicron. Thus, the total interaction energy of residues in green region of WT (Figure 5) is -268.30 kcal/mol which is higher than -367.11 kcal/mol of Omicron. In the yellow region (Figure 5), the mutations Q498R and Y505H enhance the interaction between RBD and hACE2 while N501Y weakens it. Like the Q493R mutation, the great energy change by Q498R is due to the positive charge of the R amino acid. The energy of the residues in the yellow region is 76.67 kcal/mol in WT, while for the Omicron variant it is -368.14 kcal/mol. Therefore, although Omicron has a weaker interaction in the red region, it interacts much stronger with hACE2 in other regions, which explains why K_D of Omicron is lower compared to WT, as observed in experiments of Cameroni et al and Zhang *et al*[16,17].

For heterogeneous glycans, mutations in Omicron have the same effect in the red, green and yellow regions as in the homogeneous setting (Figure 6). The contribution to the complex stability from the red region of Omicron is less than WT, while the opposite effect takes place in the green and yellow regions (Table 5). Similar to the homogeneous glycan model, the S477N mutation promotes the RBD-hACE2 association by reducing the interaction energy from -3.50 to -20.25 kcal/mol. Furthermore, the total interaction energy of the red region in Omicron (-58.73 kcal/mol) is higher than WT (-71.2 kcal/mol). In the green region, the Q493R mutation enhances the stability of the complex, since the interaction energy of 493R is -373.35 kcal/mol for Omicron versus -38.09 kcal/mol of 493Q for WT. Therefore, due to this mutation in the green region, Omicron has the interaction energy notably lower than WT (Table 5). In the yellow region, Q498R plays the same role as in the green area.

Thus, the interaction energies of residues at the RBD-hACE2 interface depend on glycan models, but both studied models exhibit the same trend, which is that compared to WT, Omicron has a higher interaction energy in the red region, while a lower energy is observed in the green and yellow regions. This suggests that due to evolution a new SARS-CoV-2 variant may have a higher binding affinity resulting in faster infection than Omicron should it has mutations in the red region.

Glycans have little effect on the RBD-hACE2 binding free energy

So far, we have discussed four systems with glycans covering both viral RBD and hACE2 PD. In order to access the influence of glycans on the binding free energy, we performed 5 independent MD runs of 200 ns each for RBD-hACE2 WT without glycans. Using the last 100 ns snapshots of the 5 MD trajectories and the MM-PBSA method, we obtained ΔG_{bind} shown in the last row of Table 3. For WT without glycans, we have ΔG_{bind} = -19.88 ± 3.27 kcal/mol, which is not differs greatly from -18.32 ± 1.62 and -17.57 ± 3.12 kcal/mol of WT surrounded by homogeneous and heterogeneous glycans, respectively. Thus, glycans have weak influence on the stability of RBD-hACE2 WT. This conclusion is expected to be valid for the Omicron variant.

Conclusions

Using MD simulation and MM-PBSA method, we obtained the binding free energy of WT and Omicron variant of SARS-CoV-2 to hACE2 PD, which shows that Omicron binds more tightly than WT. This result can be invoked to explain the high infection rate of the Omicron variant. The electrostatic interaction was found to rule the stability of the viral RBD - hACE2 PD complex. Since hACE2 PD is negatively charged, the increase in binding affinity is due in part to an increase in the overall charge of the RBD from +3e (WT) to +6e (Omicron).

The influence of the glycan models studied in this work is twofold: the per-residue interaction energies are sensitive to the glycan scheme, but the binding free energy does not depend on it. Whether this conclusion holds for other glycan models or not requires further study.

We demonstrated that N440K, T478K, E484A, Q493R, Q498R mutations play a crucial role in the high binding affinity of Omicron to human cells. After a detailed analysis of residues located at the human cell-virus interface, we predict that the emergence of a new variant with a higher infection rate compared to Omicron is still possible. Such a variant should have mutations in the red interface region indicated in Figures 5 and 6.

ASSOCIATED CONTENT

Supporting Information.

Table S1: The contributions of non-bonded interaction energy (kcal/mol) between protein-glycan, protein-protein of the hACE2-RBD complexes. **Table S2**: The ratio (%) of SASA of glycan molecules binding to hACE2, RBD in relation to total SASA. **Figure S1**: Shown are 15 mutations in the RBD of Omicron. Figure S2: Time dependence of Cα RMSD of the WT RBD-hACE2 complex with the homogeneous (Upper) and heterogeneous (Bottom) models. **Figure S3:** Time dependence of Cα RMSD of the Omicron RBD-hACE2 complex with homogeneous (upper) and heterogeneous (bottom) glycan models. **Figure S4:** Residues of RBD that have an absolute interaction energy with hACE2 ≥ 150 kcal/mol. **Figure S5:** Population of side-chain contacts formed by RBD residues with hACE2 at the interface. The results were obtained using conformations sampled over the last 100 ns of MD simulation.

Notes: The authors declare no competing financial interest.

Acknowledgements:

This work was supported by Narodowe Centrum Nauki in Poland (Grant 2019/35/B/ST4/02086), the TASK Supercomputer Center in Gdansk, PLGrid Infrastructure, Poland, Department of Science and Technology, Ho Chi Minh city (Grant 13/2020/HĐ-QPTKHCN) and the HPCC at the Institute for Computational Science and Technology, Ho Chi Minh City, Vietnam. Hoang Linh Nguyen was funded by Vingroup JSC and supported by the Master, PhD Scholarship Programme of Vingroup Innovation Foundation (VINIF), Institute of Big Data, code VINIF.2021.TS.029.

Table 1: Mutations in the S protein of the Omicron variant. Residues located in the RBD are in bold. Δ indicates deletion.

Variant	Mutations
Omicron	A67V, Δ69-70, T95I, G142D, Δ143-145, N211I, L212V, ins213-214RE, V215P, R216E, **G339D, S371L, S373P, S375F, K417N, N440K, G446S, S477N, T478K, E484A, Q493R, G496S, Q498R, N501Y, Y505H**, T547K, D614G, H655Y, N679K, P681H, N764K, D796Y, N856K, Q954H, N969K, L981F

Table 2: Dissociation constant K_D of complexes of SARS-CoV-2 variants and hACE2. References to experimental works are given.

Variant	K_D (nM)
Wildtype	60.0 ± 1.4[16], 13.20[17], 1.66 ± 0.84[18], 22.0[19]
Omicron	25.3 ± 1.2[16], 8.85[17], 27.0 ± 340.0[18]

Glycan model	Variant	electrostatic	Van der Waals	PB	SA	entropy	ΔG_{bind}
Homo glycan model	WT	-856.33± 3.63	-152.18 ± 9.90	990.29 ± 15.15	-24.27 ± 1.50	24.18 ± 1.29	-18.32 ± 1.62
	Omicron	-1645.73 ± 15.33	-144.86 ± 11.15	1752.76 ± 31.90	-23.58 ± 1.50	31.20 ± 3.06	-30.21 ± 4.48
Hetero glycan model	WT	-952.72 ± 17.20	-159.62 ± 6.01	1086.07 ± 14.75	-26.17 ± 0.80	34.87 ± 3.41	-17.57 ± 3.12
	Omicron	-1909.30 ± 18.80	-153.72 ± 6.09	2029.94 ± 40.79	-25.84 ± 2.49	30.94 ± 2.37	-27.97 ± 2.91
No glycans	WT	-778.71 ± 25.20	-93.71 ± 5.12	842.50 ± 27.92	-14.74 ± 0.40	24.78 ± 3.34	-19.88 ± 3.27

Table 3: Binding free energy (kcal/mol) of WT and Omicron variant. Results were obtained using the MM-PBSA method and snapshots of the last 100 ns from 5 MD runs. Errors are standard deviations. The last row refers to WT without glycans.

Table 4: Residues of RBD that have an absolute interaction energy with hACE2 PD ≥ 150 kcal/mol.

Glycan model	System	Residues that have an interaction energy ≤ -150 kcal/mol	Residues that have an interaction energy ≥150 kcal/mol
Homogeneous	WT	R319, R346, R355, K356, R357, N360, P384, K386, R403, R408, K417, N422, K424, P426, L441, G446, N450, L452, L455, R457, K462, N487, L492, S494, G496, Q506	T323, N334, E340, N354, N370, S373, T385, N394, E406, D420, D427, D428, T430, N437, D442, Y451, P463, E484, C488, Y495, Q498, E516, T523, P527
	Omicron	R319, R346, R355, K378, R403, R408, K424, K440, K444, R454, R457, K458, K462, R466, K478, R493, R498, R509	D339, E340, D398, D405, E406, D420, D427, D428, D442, E465, D467, E471
Heterogeneous	WT	R319, R346, R355, K356, R357, K378, K386, R403, R408, K417, K424, K444, R454, R457, K458, K462, R466, R509	E340, D364, D389, D398, D405, E406, D420, D427, D428, D442, E465, D467, E471, E484, E516, P527
	Omicron	R319, R346, R355, K356, R357, K378, K386, R403, R408, K424, K440, K444, R454, R457, K458, K462, R466, K478, R493, R498, R509	D339, E340, D364, D389, D398, D405, E406, D420, D427, D428, D442, D465, E467, D471, E516, P527

Table 5: The average total interaction energy, total hydropathy[40] and total charge of RBD residues that have a side-chain contact with hACE2. Data are divided into 3 regions red, green, and yellow.

Glycan model	Variant	region	average total energy (kcal/	hydropathy	Charge (e)

			mol)		
Homogeneous	WT	red	-217.85	3.1	0
		green	-268.30	-0.1	0
		yellow	76.67	-6.4	0
	Omicron	red	-81.28	-2.1	0
		green	-367.11	-1.5	1
		yellow	-368.14	-6.7	1
Heterogeneous	WT	red	-71.20	-1.7	0
		green	-34.70	-2.2	0
		yellow	-96.94	-9.1	0
	Omicron	red	-58.73	-5.2	0
		green	-357.97	-1.5	1
		yellow	-453.73	-6.7	1

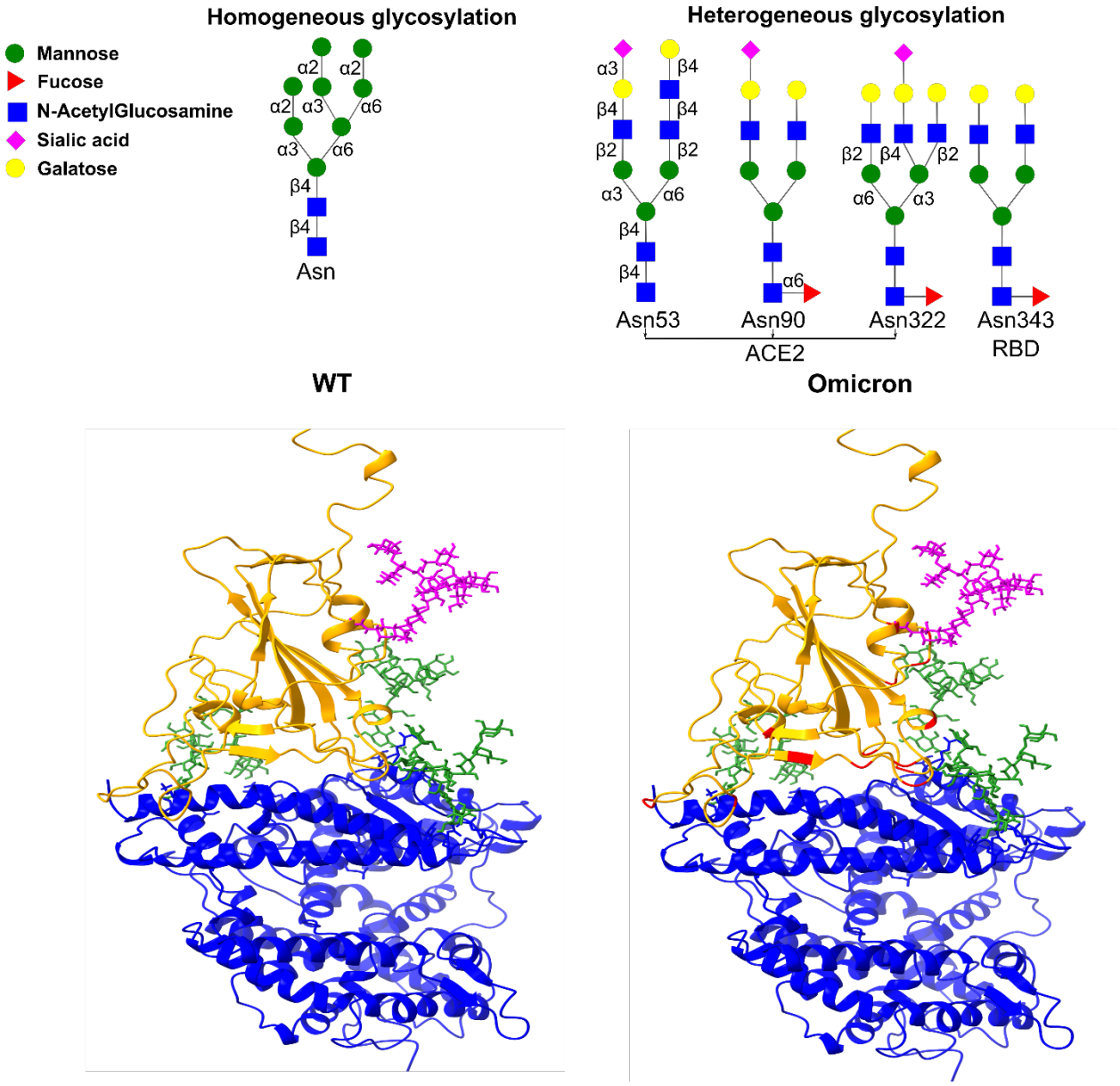

Figure 1: (Upper) Glycan models used in this work. Magenta refers to the glycan flanking RBD, while green refers to the three glycans surrounding hACE2. (Bottom) PDB structure of the WT RBD-hACE2 PD and Omicron RBD-hACE2 PD complexes. RBD is highlighted in orange, hACE2 in blue, and mutations in red.

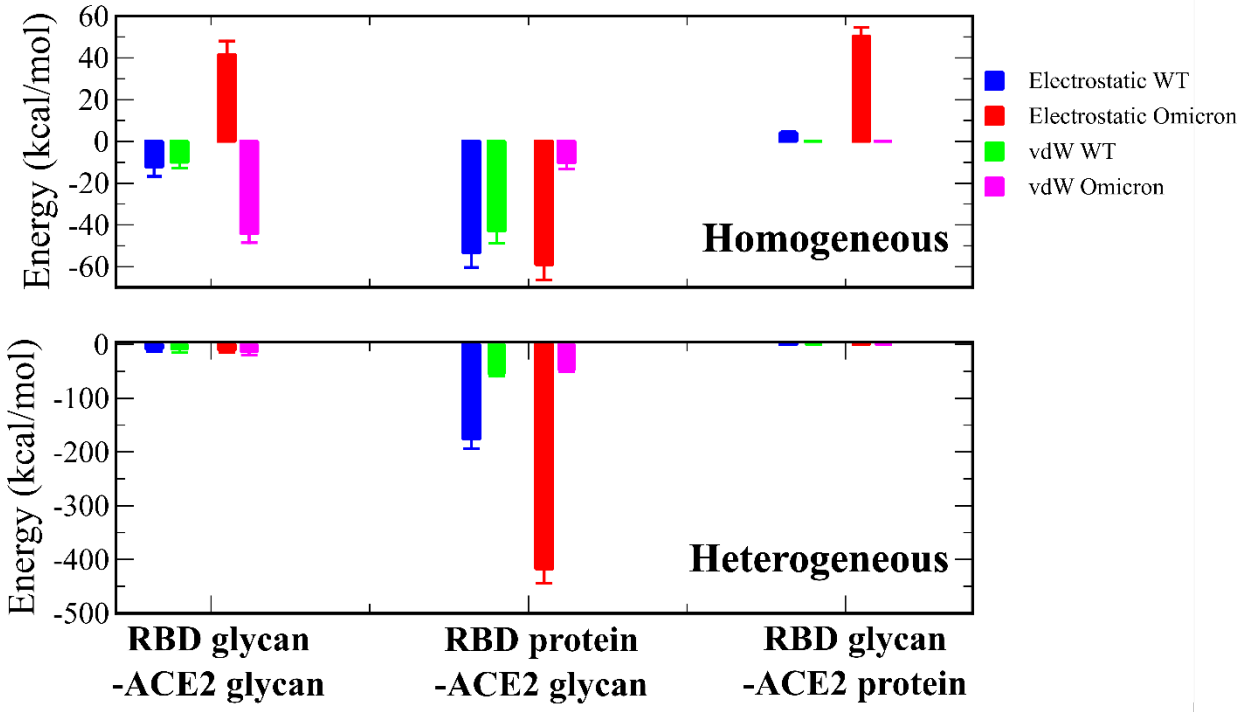

Figure 2: Energy of RBD glycan-hACE2 glycan, RBD protein-hACE2 glycan and RBD glycan-hACE2 protein interactions.

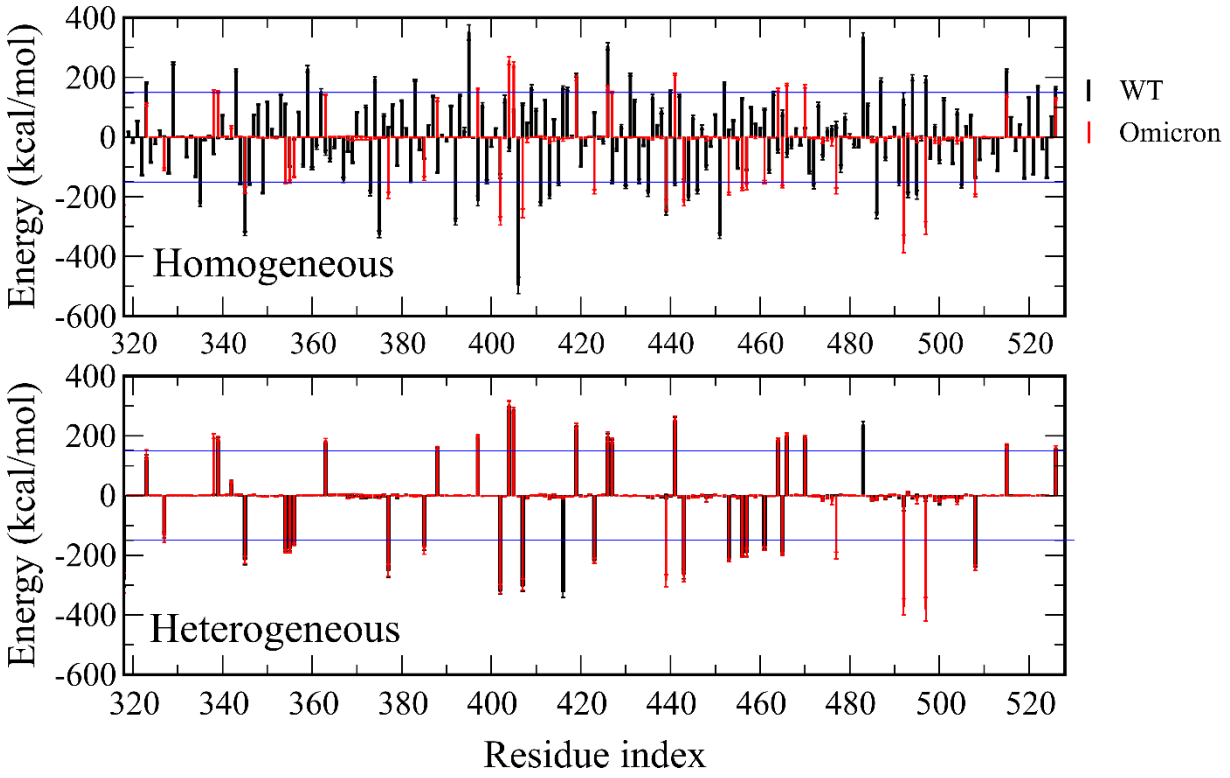

Figure 3: Interaction energy for individual residues. The blue line refers to 150 and -150 kcal/mol.

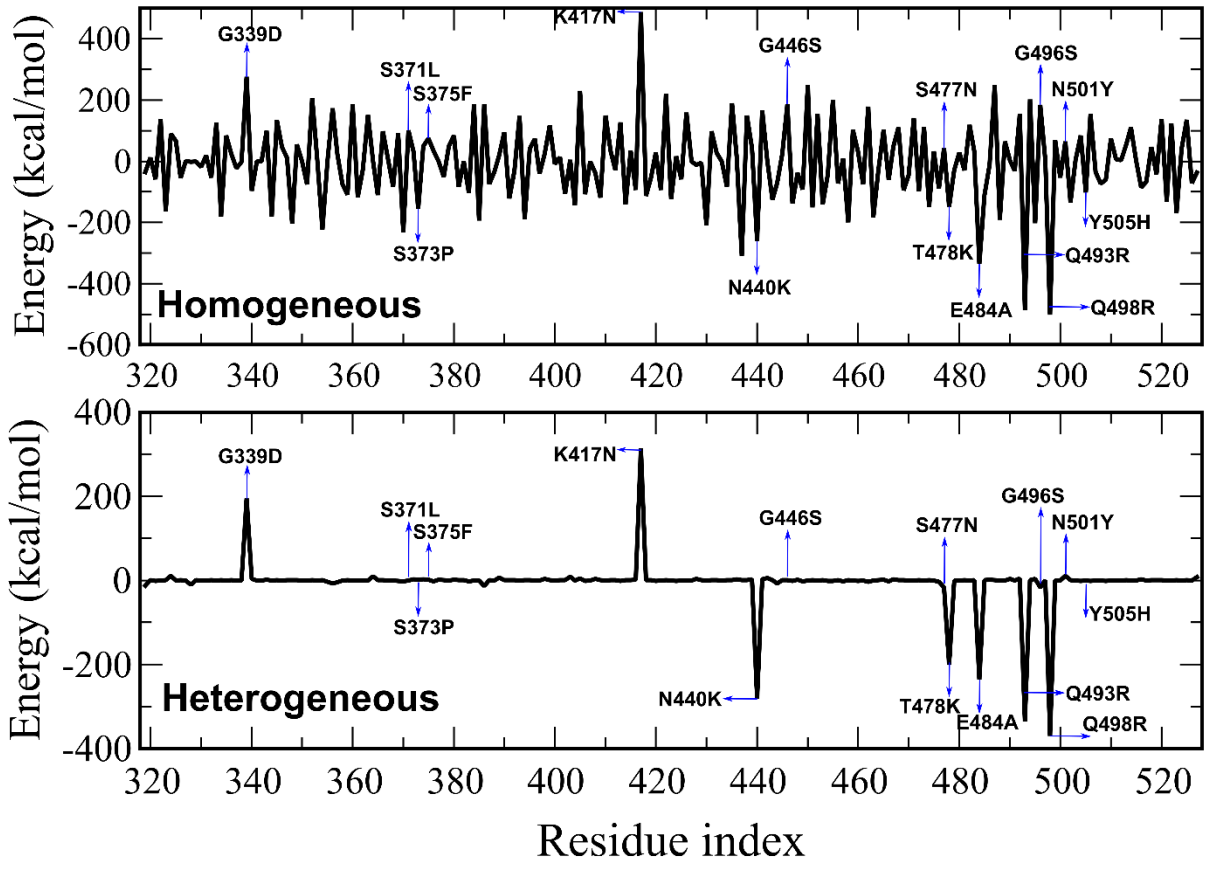

Figure 4: The difference between the interaction energies of Omicron and WT residues ($E_{\text{Omicron}} - E_{\text{WT}}$) for homogeneous (Upper) and heterogeneous (Bottom) glycan models.

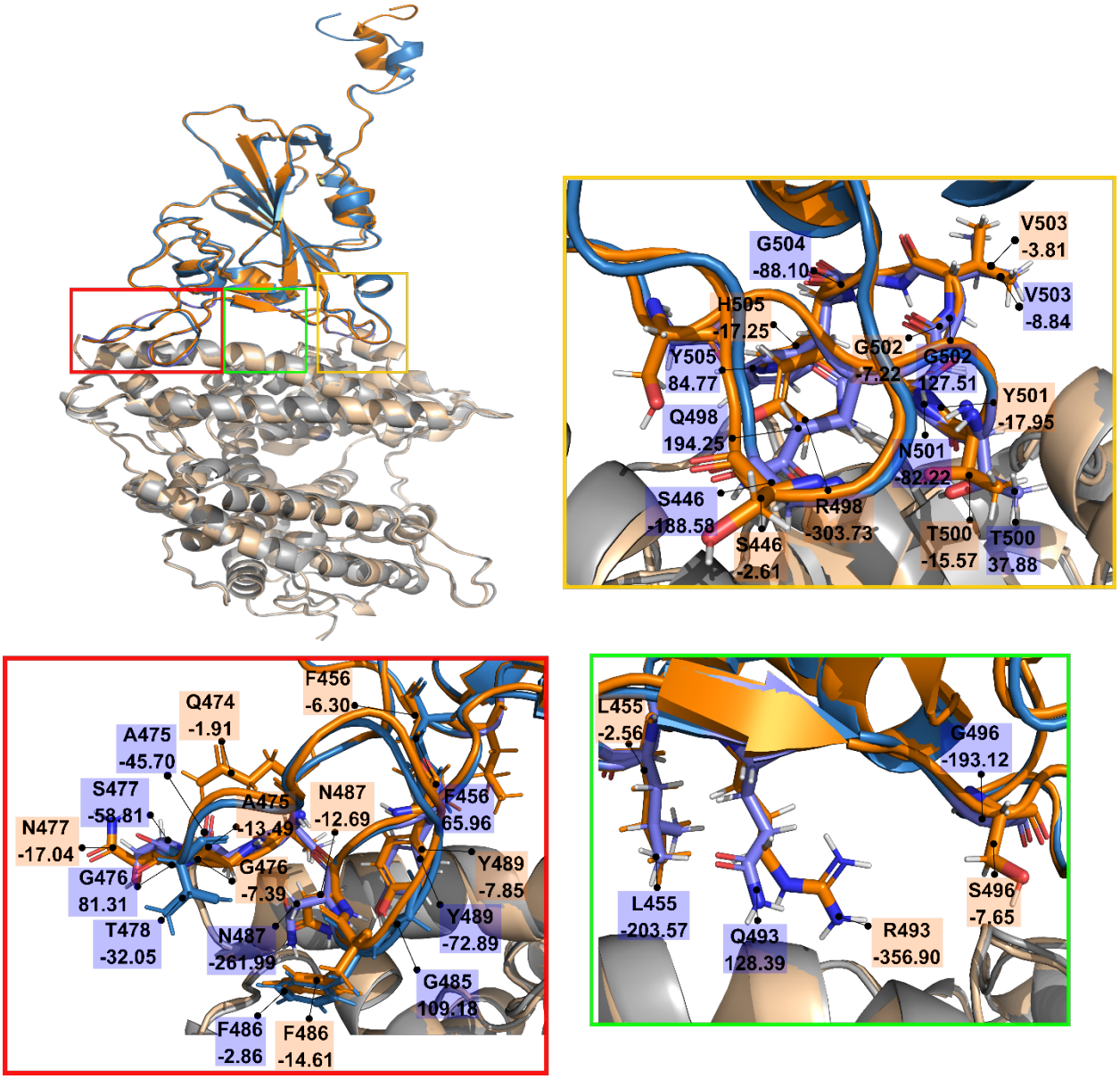

Figure 5: The alignment of the WT RBD (blue)-hACE2 (gray) and Omicron RBD (orange)-hACE2 (wheat) complexes. For clarity glycans have been removed. RBD residues that have a side chain contact with hACE2 residues are enclosed in large red, green and yellow boxes for the homogeneous glycan model. The label of RBD residues and their interaction energy with hACE2 are shown in small blue and orange rectangles for WT and Omicron, respectively.

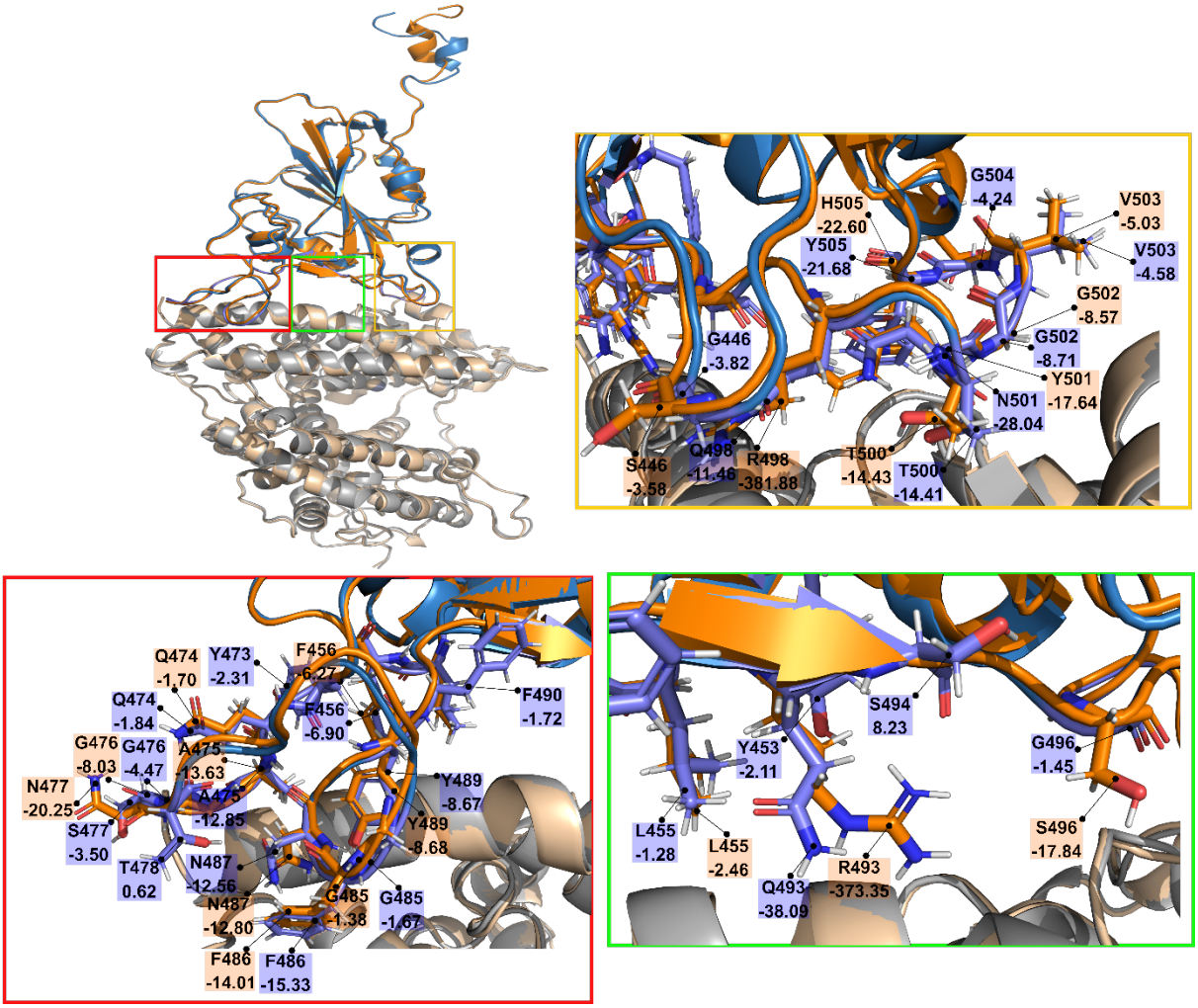

Figure 6: The same as in Figure 5 but for the heterogeneous glycan model.

TOC Graphic

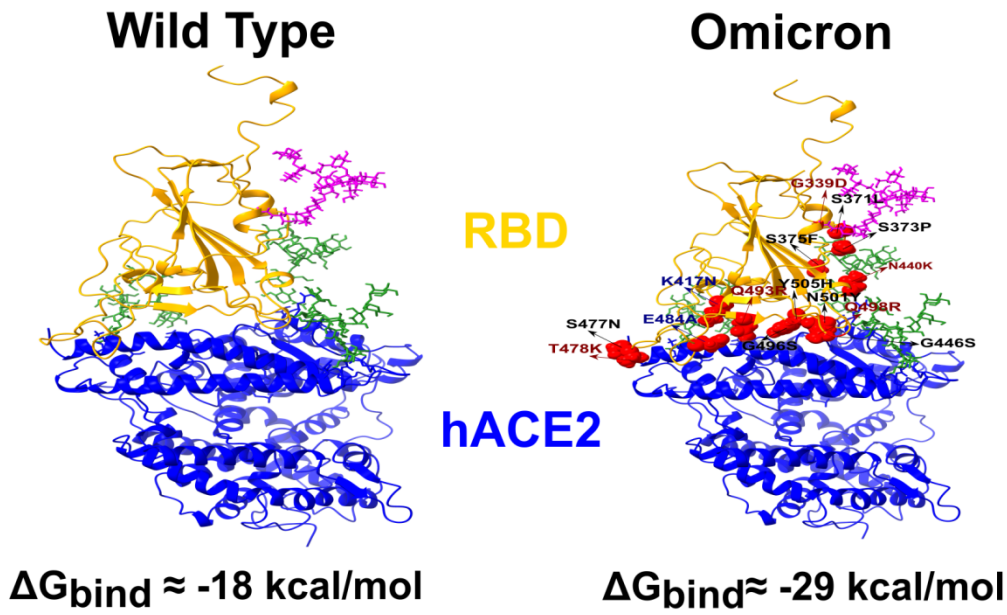
Wild Type
Omicron
RBD
hACE2
G339D
S371L
S373P
S375F
N440K
K417N
Y505H
Q493R
N501Y
Q498R
S477N
E484A
T478K
G496S
G446S
ΔG$_{bind}$ ≈ -18 kcal/mol
ΔG$_{bind}$≈ -29 kcal/mol

References

(1) Gorbalenya, A. E.; Baker, S. C.; Baric, R. S.; de Groot, R. J.; Drosten, C.; Gulyaeva, A. A.; Haagmans, B. L.; Lauber, C.; Leontovich, A. M.; Neuman, B. W.; Penzar, D.; Perlman, S.; Poon, L. L. M.; Samborskiy, D. V.; Sidorov, I. A.; Sola, I.; Ziebuhr, J.; Coronaviridae Study Group of the International Committee on Taxonomy of, V. The species Severe acute respiratory syndrome-related coronavirus: classifying 2019-nCoV and naming it SARS-CoV-2. *Nature Microbiology* **2020**, *5*, 536-544.

(2) Dong, E.; Du, H.; Gardner, L. An interactive web-based dashboard to track COVID-19 in real time. *The Lancet infectious diseases* **2020**, *20*, 533-534.

(3) Yang, J.; Petitjean, S. J.; Koehler, M.; Zhang, Q.; Dumitru, A. C.; Chen, W.; Derclaye, S.; Vincent, S. P.; Soumillion, P.; Alsteens, D. Molecular interaction and inhibition of SARS-CoV-2 binding to the ACE2 receptor. *Nat. Commun.* **2020**, *11*, 1-10.

(4) Iyer, A. S.; Jones, F. K.; Nodoushani, A.; Kelly, M.; Becker, M.; Slater, D.; Mills, R.; Teng, E.; Kamruzzaman, M.; Garcia-Beltran, W. F. Persistence and decay of human antibody responses to the receptor binding domain of SARS-CoV-2 spike protein in COVID-19 patients. *Science immunology* **2020**, *5*.

(5) Wang, P.; Nair, M. S.; Liu, L.; Iketani, S.; Luo, Y.; Guo, Y.; Wang, M.; Yu, J.; Zhang, B.; Kwong, P. D.; Graham, B. S.; Mascola, J. R.; Chang, J. Y.; Yin, M. T.; Sobieszczyk, M.; Kyratsous, C. A.; Shapiro, L.; Sheng, Z.; Huang, Y.; Ho, D. D. Antibody resistance of SARS-CoV-2 variants B.1.351 and B.1.1.7. *Nature* **2021**, *593*, 130-135.

(6) Premkumar, L.; Segovia-Chumbez, B.; Jadi, R.; Martinez, D. R.; Raut, R.; Markmann, A. J.; Cornaby, C.; Bartelt, L.; Weiss, S.; Park, Y.; Edwards, C. E.; Weimer, E.; Scherer, E. M.; Rouphael, N.; Edupuganti, S.; Weiskopf, D.; Tse, L. V.; Hou, Y. J.; Margolis, D.; Sette, A.; Collins, M. H.; Schmitz, J.; Baric, R. S.; Silva, A. M. d. The receptor-binding domain of the viral spike protein is an immunodominant and highly specific target of antibodies in SARS-CoV-2 patients. *Science Immunology* **2020**, *5*, eabc8413.

(7) Jackson, C. B.; Farzan, M.; Chen, B.; Choe, H. Mechanisms of SARS-CoV-2 entry into cells. *Nature Reviews Molecular Cell Biology* **2022**, *23*, 3-20.

(8) Lan, J.; Ge, J.; Yu, J.; Shan, S.; Zhou, H.; Fan, S.; Zhang, Q.; Shi, X.; Wang, Q.; Zhang, L.; Wang, X. Structure of the SARS-CoV-2 spike receptor-binding domain bound to the ACE2 receptor. *Nature* **2020**, *581*, 215-220.

(9) Shang, J.; Ye, G.; Shi, K.; Wan, Y.; Luo, C.; Aihara, H.; Geng, Q.; Auerbach, A.; Li, F. Structural basis of receptor recognition by SARS-CoV-2. *Nature* **2020**, *581*, 221-224.

(10) Organization, W. H. Classification of Omicron (B. 1.1. 529): SARS-CoV-2 variant of concern. *November* **2021**, *26*, 2021.

(11) Gao, S.-J.; Guo, H.; Luo, G. Omicron variant (B.1.1.529) of SARS-CoV-2, a global urgent public health alert! *J. Med. Virol.*, *n/a*.

(12) Tareq, A. M.; Emran, T. B.; Dhama, K.; Dhawan, M.; Tallei, T. E. Impact of SARS-CoV-2 delta variant (B.1.617.2) in surging second wave of COVID-19 and efficacy of vaccines in tackling the ongoing pandemic. *Human Vaccines & Immunotherapeutics* **2021**, 1-2.

(13) Grant, R.; Charmet, T.; Schaeffer, L.; Galmiche, S.; Madec, Y.; Von Platen, C.; Chény, O.; Omar, F.; David, C.; Rogoff, A.; Paireau, J.; Cauchemez, S.; Carrat, F.; Septfons, A.; Levy-Bruhl, D.; Mailles, A.; Fontanet, A. Impact of SARS-CoV-2 Delta variant on incubation, transmission settings and vaccine effectiveness: Results from a nationwide case-control study in France. *The Lancet Regional Health - Europe* **2021**, 100278.

(14) Pouwels, K. B.; Pritchard, E.; Matthews, P. C.; Stoesser, N.; Eyre, D. W.; Vihta, K.-D.; House, T.; Hay, J.; Bell, J. I.; Newton, J. N.; Farrar, J.; Crook, D.; Cook, D.; Rourke, E.; Studley, R.; Peto, T. E. A.; Diamond, I.; Walker, A. S. Effect of Delta variant on viral burden and vaccine effectiveness against new SARS-CoV-2 infections in the UK. *Nat. Med.* **2021**, *27*, 2127-2135.

(15) Karim, S. S. A.; Karim, Q. A. Omicron SARS-CoV-2 variant: a new chapter in the COVID-19 pandemic. *Lancet* **2021**, *398*, 2126-2128.

(16) Cameroni, E.; Bowen, J. E.; Rosen, L. E.; Saliba, C.; Zepeda, S. K.; Culap, K.; Pinto, D.; VanBlargan, L. A.; De Marco, A.; di Iulio, J.; Zatta, F.; Kaiser, H.; Noack, J.; Farhat, N.; Czudnochowski, N.; Havenar-Daughton, C.; Sprouse, K. R.; Dillen, J. R.; Powell, A. E.; Chen, A.; Maher, C.; Yin, L.; Sun, D.; Soriaga, L.; Bassi, J.; Silacci-Fregni, C.; Gustafsson, C.; Franko, N. M.; Logue, J.; Iqbal, N. T.; Mazzitelli, I.; Geffner, J.; Grifantini, R.; Chu, H.; Gori, A.; Riva, A.; Giannini, O.; Ceschi, A.; Ferrari, P.; Cippà, P. E.; Franzetti-Pellanda, A.; Garzoni, C.; Halfmann, P. J.; Kawaoka, Y.; Hebner, C.; Purcell, L. A.; Piccoli, L.; Pizzuto, M. S.; Walls, A. C.; Diamond, M. S.; Telenti, A.; Virgin, H. W.; Lanzavecchia, A.; Snell, G.; Veesler, D.; Corti, D. Broadly neutralizing antibodies overcome SARS-CoV-2 Omicron antigenic shift. *Nature* **2021**.

(17) Zhang, X.; Wu, S.; Wu, B.; Yang, Q.; Chen, A.; Li, Y.; Zhang, Y.; Pan, T.; Zhang, H.; He, X. SARS-CoV-2 Omicron strain exhibits potent capabilities for immune evasion and viral entrance. *Signal Transduction and Targeted Therapy* **2021**, *6*, 430.

(18) Wu, L.; Zhou, L.; Mo, M.; Liu, T.; Wu, C.; Gong, C.; Lu, K.; Gong, L.; Zhu, W.; Xu, Z. SARS-CoV-2 Omicron RBD shows weaker binding affinity than the currently dominant Delta variant to human ACE2. *Signal Transduction and Targeted Therapy* **2022**, *7*, 8.

(19) Chan, K. K.; Dorosky, D.; Sharma, P.; Abbasi, S. A.; Dye, J. M.; Kranz, D. M.; Herbert, A. S.; Procko, E. Engineering human ACE2 to optimize binding to the spike protein of SARS coronavirus 2. *Science* **2020**, *369*, 1261-1265.

(20) Chen, J.; Wang, R.; Gilby, N. B.; Wei, G.-W. Omicron Variant (B.1.1.529): Infectivity, Vaccine Breakthrough, and Antibody Resistance. *J. Chem. Inf. Model.* **2022**.

(21) Kumar, S.; Thambiraja, T. S.; Karuppanan, K.; Subramaniam, G. Omicron and Delta variant of SARS-CoV-2: A comparative computational study of spike protein. *J. Med. Virol.*, *n/a*.

(22) Omotuyi, O.; Olubiyi, O.; Nash, O.; Afolabi, E.; Oyinloye, B.; Fatumo, S.; Femi-Oyewo, M.; Bogoro, S. SARS-CoV-2 Omicron spike glycoprotein receptor binding domain exhibits super-binder ability with ACE2 but not convalescent monoclonal antibody. *Computers in Biology and Medicine* **2022**, *142*, 105226.

(23) Wang, Q.; Zhang, Y.; Wu, L.; Niu, S.; Song, C.; Zhang, Z.; Lu, G.; Qiao, C.; Hu, Y.; Yuen, K.-Y.; Wang, Q.; Zhou, H.; Yan, J.; Qi, J. Structural and Functional Basis of SARS-CoV-2 Entry by Using Human ACE2. *Cell* **2020**, *181*, 894-904.e899.

(24) Shajahan, A.; Archer-Hartmann, S.; Supekar, N. T.; Gleinich, A. S.; Heiss, C.; Azadi, P. Comprehensive characterization of N- and O- glycosylation of SARS-CoV-2 human receptor angiotensin converting enzyme 2. *Glycobiology* **2020**, *31*, 410-424.

(25) Watanabe, Y.; Allen, J. D.; Wrapp, D.; McLellan, J. S.; Crispin, M. Site-specific glycan analysis of the SARS-CoV-2 spike. *Science* **2020**, *369*, 330-333.

(26) Tian, C.; Kasavajhala, K.; Belfon, K. A. A.; Raguette, L.; Huang, H.; Migues, A. N.; Bickel, J.; Wang, Y.; Pincay, J.; Wu, Q.; Simmerling, C. ff19SB: Amino-Acid-Specific

Protein Backbone Parameters Trained against Quantum Mechanics Energy Surfaces in Solution. *J Chem Theory Comput* **2020**, *16*, 528-552.

(27) Kirschner, K. N.; Lins, R. D.; Maass, A.; Soares, T. A. A Glycam-Based Force Field for Simulations of Lipopolysaccharide Membranes: Parametrization and Validation. *J. Chem. Theory Comput.* **2012**, *8*, 4719-4731.

(28) Izadi, S.; Anandakrishnan, R.; Onufriev, A. V. Building Water Models: A Different Approach. *The Journal of Physical Chemistry Letters* **2014**, *5*, 3863-3871.

(29) Bussi, G.; Donadio, D.; Parrinello, M. Canonical sampling through velocity rescaling. *J. Chem. Phys.* **2007**, *126*, 014101.

(30) Parrinello, M.; Rahman, A. Polymorphic transitions in single crystals: A new molecular dynamics method. *Journal of Applied Physics* **1981**, *52*, 7182-7190.

(31) Darden, T.; Perera, L.; Li, L.; Pedersen, L. New tricks for modelers from the crystallography toolkit: the particle mesh Ewald algorithm and its use in nucleic acid simulations. *Structure* **1999**, *7*, R55-R60.

(32) Li, L.; Li, C.; Sarkar, S.; Zhang, J.; Witham, S.; Zhang, Z.; Wang, L.; Smith, N.; Petukh, M.; Alexov, E. DelPhi: a comprehensive suite for DelPhi software and associated resources. *BMC Biophys* **2012**, *5*, 9.

(33) Eisenhaber, F.; Lijnzaad, P.; Argos, P.; Sander, C.; Scharf, M. The double cubic lattice method: Efficient approaches to numerical integration of surface area and volume and to dot surface contouring of molecular assemblies. *J. Comput. Chem.* **1995**, *16*, 273-284.

(34) Duan, L.; Liu, X.; Zhang, J. Z. Interaction Entropy: A New Paradigm for Highly Efficient and Reliable Computation of Protein-Ligand Binding Free Energy. *J Am Chem Soc* **2016**, *138*, 5722-5728.

(35) Williams, A. H.; Zhan, C.-G. Fast Prediction of Binding Affinities of the SARS-CoV-2 Spike Protein Mutant N501Y (UK Variant) with ACE2 and Miniprotein Drug Candidates. *J. Phys. Chem. B* **2021**, *125*, 4330-4336.

(36) Zhang, Y.; He, X.; Zhai, J.; Ji, B.; Man, V. H.; Wang, J. In silico binding profile characterization of SARS-CoV-2 spike protein and its mutants bound to human ACE2 receptor. *Briefings in Bioinformatics* **2021**, *22*.

(37) Nissley, D. A.; Vu, Q. V.; Trovato, F.; Ahmed, N.; Jiang, Y.; Li, M. S.; O'Brien, E. P. Electrostatic Interactions Govern Extreme Nascent Protein Ejection Times from Ribosomes and Can Delay Ribosome Recycling. *Journal of the American Chemical Society* **2020**, *142*, 6103-6110.

(38) Nguyen, H. L.; Lan, P. D.; Thai, N. Q.; Nissley, D. A.; O'Brien, E. P.; Li, M. S. Does SARS-CoV-2 Bind to Human ACE2 Stronger Than SARS-CoV? *J. Phys. Chem. B* **2020**.

(39) Mehdipour, A. R.; Hummer, G. Dual nature of human ACE2 glycosylation in binding to SARS-CoV-2 spike. *Proc. Natl. Acad. Sci.* **2021**, *118*, e2100425118.

(40) Kyte, J.; Doolittle, R. F. A simple method for displaying the hydropathic character of a protein. *Journal of Molecular Biology* **1982**, *157*, 105-132.